Physics

Physics Research Publications

Purdue University *Year* 2010

Refractive index and dielectric constant evolution of ultra-thin gold from clusters to films

X. F. Wang K. P. Chen

M. Zhao D. D. Nolte

Refractive index and dielectric constant evolution of ultra-thin gold from clusters to films

Xuefeng Wang,[1] Kuo-ping Chen,[2] Ming Zhao,[1] and David D. Nolte[1]

[1]*Department of Physics, Purdue University, West Lafayette, Indiana 47907, USA*
[2] *Department of Electrical and Computer Engineering, Purdue University, West Lafayette, Indiana 47907, USA*
**nolte@physics.purdue.edu*

Abstract: Using high-speed picometrology, the complete cluster-to-film dielectric trajectories of ultra-thin gold films on silica are measured at 488 nm and 532 nm wavelengths for increasing mass-equivalent thickness from 0.2 nm to 10 nm. The trajectories are parametric curves on the complex dielectric plane that consist of three distinct regimes with two turning points. The thinnest regime (0.2 nm – 0.6 nm) exhibits increasing dipole density up to the turning point for the real part of the dielectric function at which the clusters begin to acquire metallic character. The mid-thickness regime (0.6 nm ~2 nm) shows a linear trajectory approaching the turning point for the imaginary part of the dielectric function. The third regime, from 2 nm to 10 nm, clearly displays the Drude circle, with no observable feature at the geometric percolation transition.

OCIS codes: (120.3940) Instrument, measurement and metrology; (240.0240) Optics at surfaces; (310.6860) Thin film, optical properties; (260.3910) metal optics.

References and links

1. E. Ozbay, "Plasmonics: merging photonics and electronics at nanoscale dimensions," Science **311**(5758), 189–193 (2006).
2. R. B. Laibowitz, and Y. Gefen, "Dynamic Scaling near the Percolation-Threshold in Thin Au Films," Phys. Rev. Lett. **53**(4), 380–383 (1984).
3. J. J. Tu, C. C. Homes, and M. Strongin, "Optical properties of ultrathin films: evidence for a dielectric anomaly at the insulator-to-metal transition," Phys. Rev. Lett. **90**(1), 017402 (2003).
4. A. Gray, M. Balooch, S. Allegret, S. De Gendt, and W. E. Wang, "Optical detection and characterization of graphene by broadband spectrophotornetry," J. Appl. Phys. **104**(5), 053109 (2008).
5. P. Grosse, and V. Offermann, "Analysis of Reflectance Data Using the Kramers-Kronig Relations," Appl. Phys., A Mater. Sci. Process. **52**(2), 138–144 (1991).
6. D. A. Crandles, F. Eftekhari, R. Faust, G. S. Rao, M. Reedyk, and F. S. Razavi, "Kramers-Kronig-constrained variational dielectric fitting and the reflectance of a thin film on a substrate," Appl. Opt. **47**(23), 4205–4211 (2008).
7. M. Hövel, B. Gompf, and M. Dressel, "Dielectric properties of ultrathin metal films around the percolation threshold," Phys. Rev. B **81**(3), 035402 (2010).
8. F. L. McCrackin, E. Passaglia, R. R. Stromberg, and H. Steinber, "Measurememt of Thickness and Refractive Index of Very Thin Films and Optical Properties of Surfaces by Ellipsometry," J. Res. Natl. Bur. Stand. **A 67**, 363–377 (1963).
9. R. J. Archer, "Determination of Properties of Films on Silicon by Method of Ellipsometry," J. Opt. Soc. Am. **52**(9), 970–977 (1962).
10. M. Yamamoto, and T. Namioka, "In situ ellipsometric study of optical properties of ultrathin films," Appl. Opt. **31**(10), 1612–1621 (1992).
11. X. Wang, M. Zhao, and D. D. Nolte, "Common-path interferometric detection of protein monolayer on the BioCD," Appl. Opt. **46**(32), 7836–7849 (2007).
12. X. F. Wang, Y. P. Chen, and D. D. Nolte, "Strong anomalous optical dispersion of graphene: complex refractive index measured by Picometrology," Opt. Express **16**(26), 22105–22112 (2008).
13. O. S. Heavens, *Optical Properties of thin solid films* (Academic Press Inc., New York, 1955), p. 66~80.
14. V. M. Shalaev, *Nonlinear Optics of Random Media: Fractal Composites and Metal-Dielectric Films*, Springer Tracts in Modern Physics (Berlin Heidelberg, 2000).
15. H. Y. Li, S. M. Zhou, J. Li, Y. L. Chen, S. Y. Wang, Z. C. Shen, L. Y. Chen, H. Liu, and X. X. Zhang, "Analysis of the drude model in metallic films," Appl. Opt. **40**(34), 6307–6311 (2001).
16. F. Abeles, *Optical Properties of Solids* (North-Holland, Amsterdam, 1972), p. 103.
17. M. Walther, D. G. Cooke, C. Sherstan, M. Hajar, M. R. Freeman, and F. A. Hegmann, "Terahertz conductivity of thin gold films at the metal-insulator percolation transition," Phys. Rev. B **76**(12), 125408 (2007).

#135785 - $15.00 USD Received 28 Sep 2010; revised 25 Oct 2010; accepted 26 Oct 2010; published 12 Nov 2010

18. U. Kreibig, and C. V. Fragstein, "Limitation of Electron Mean Free Path in Small Silver Particles," Z. Naturforsch. B **224**, 307–323 (1969).
19. M. G. Blaber, M. D. Arnold, and M. J. Ford, "Search for the Ideal Plasmonic Nanoshell: The Effects of Surface Scattering and Alternatives to Gold and Silver," J. Phys. Chem. C **113**(8), 3041–3045 (2009).
20. C. Noguez, and C. E. Roman-Velazquez, "Dispersive force between dissimilar materials: Geometrical effects," Phys. Rev. B **70**(19), 195412 (2004).
21. M. Kreiter, S. Mittler, W. Knoll, and J. R. Sambles, "Surface plasmon-related resonances on deep and asymmetric gold gratings," Phys. Rev. B **65**(12), 125415 (2002).
22. T. Zychowicz, J. Krupka, and J. Mazierska, "Measurements of Conductivity of Thin Gold Films at Microwave Frequencies Employing Resonant Techniques," Proceedings of Asia-Pacific Microwave Conference (2006).

1. Introduction

The noble metals lie at the interface between optical and electronic physics [1]. As the scale of metal nanophotonic and plasmonic elements shrink, metallic behavior becomes size dependent, and thin layers fragment into clusters that have different optical properties than the bulk [2,3]. Despite the importance of gold as an archetypical metal and its importance for photonic applications, there has been no study revealing the continuous cluster-to-film-to-bulk transition of the complex refractive index $\tilde{n}$ and dielectric constant $\tilde{\varepsilon}$, especially when the metal film average thickness is below 2 nm. The ultra-thin regime is inaccessible to current techniques for thin film optical studies. Because $\tilde{n}$ is complex with two variables (real part and imaginary part), a one-parameter measurement cannot acquire the full information needed to calculate $\tilde{n}$. Traditional methods select two or more photonic states of the probe light, such as wavelength, polarization or incidence angle [4] to execute multiple-parameter measurements. For example, spectral reflectometry measures the reflectance change caused by the thin film in a broad wavelength range and uses the Kramers-Kronig relation to find $\tilde{n}$ [5–7]. Ellipsometry measures $\tilde{n}$ by monitoring reflectances at two different polarization states of oblique-incident light [8,9]. However, changing the photonic state of the probe light potentially limits the measurement of $\tilde{n}$ because of optical dispersion or anisotropy which occurs for sub-nanometer metal films. These consequences limit the validity of traditional methods in the ultra-thin regime. For example, ellipsometric measurements become erratic when the gold film thickness is below 6 nm [7,10].

We have developed interferometric picometrology which measures $\tilde{n}$ using a single photonic state (single wavelength, single polarization and normal incidence) [11]. Picometrology monitors the complex change of the normal-incidence reflection coefficient $\tilde{r}$ instead of reflectance R to calculate $\tilde{n}$ of the film by analyzing the far-field diffraction of a patterned film in a single measurement which efficiently excludes errors introduced by multiple measurements. The change of $\tilde{r}$ is obtained by monitoring the change of the far-field diffraction pattern as the focal spot scans over the edge of a thin film. The phase change of $\varphi(\tilde{r})$ is obtained by monitoring the spatial asymmetry of the diffraction pattern, and the amplitude is obtained by monitoring the overall intensity. The scanning system shown in Fig. 1a is employed to perform the picometrology measurement. Both the modulus and the phase change of $\tilde{r}$ caused by the thin film are acquired using a split detector that simultaneously monitors intensities and asymmetries of the reflected beam. The split detector is located on the Fourier plane and consists of two semi-circular halves that contribute signals A and B. The intensity (I) signal of the diffraction pattern is acquired as I = A + B, and the spatial asymmetry signal (phase contrast, PC) is acquired as PC = A-B. Typical I and PC channel signals are shown in Fig. 1b. The complex index $\tilde{n}$ is calculated using the picometrology equation [12]

$$(\tilde{n}^2-1)\frac{(1+\tilde{r})^2}{\tilde{r}}\frac{2\pi d}{\lambda}=3.565A\left[i^{PC}(x)\right]+A\left[i^{I}(x)\right]j, \qquad (1)$$

where $\tilde{r}$ is the reflection coefficient of the bare substrate, λ is the free space wavelength, $i^{I}(x)$ and $i^{PC}(x)$ are the normalized signals of the I and PC channels, and $A\left[i^{I}(x)\right]$ and

#135785 - $15.00 USD Received 28 Sep 2010; revised 25 Oct 2010; accepted 26 Oct 2010; published 12 Nov 2010

$A\left[i^{PC}(x)\right]$ represent the amplitudes of $i^{I}(x)$ and $i^{PC}(x)$. The mass-equivalent thickness is defined as $d=\sigma_m/\rho_m$ where σ_m is the surface mass density measured by a quartz crystal monitor, and ρ_m is the molecular mass density of gold. The platform consists of a spinner and a linear stage to produce a two-dimensional picometrology scan. We previously applied this system to measure anomalous dispersion of graphene [12].

2. Experiments

To study $\tilde{n}$ and $\tilde{\varepsilon}$ of gold at arbitrary thicknesses in the range of 0~10 nm, we created gold samples with average gold film thicknesses that increased continuously and linearly from 0 to 10 nm along the y-direction (Fig. 1b) on a single substrate. This was achieved by a metal evaporator modified by attaching a stepper-motor-controlled shutter between the evaporation source and the silicon chip. The shutter moves with constant speed and exposes the chip surface continuously and incrementally during evaporation. The gold deposition rate in these experiments was 0.2 nm/s, and the silicon chip was at room temperature (300 K). The optical study of gold with mass-equivalent thicknesses from 0 to 10 nm is performed on a single chip to eliminate the error due to variations among different chips. Because picometrology is based on Gaussian beam diffraction from the edge of a film, the gold film is deposited in a stripe pattern (Fig. 1b) fabricated using photolithography. The periodic pattern along the x-direction provides multiple edges and improves the detection sensitivity. The substrate is a silicon chip with a 134 nm SiO_2 layer (measured by a spectroscopic analysis of the reflectance) that is chosen to give nominally equal I and PC signals in Eq. (1). Prior to gold evaporation, the substrate was cleaned by acetone in a sonic bath for 15 min and rinsed with methanol and deionized water and dried with a nitrogen stream.

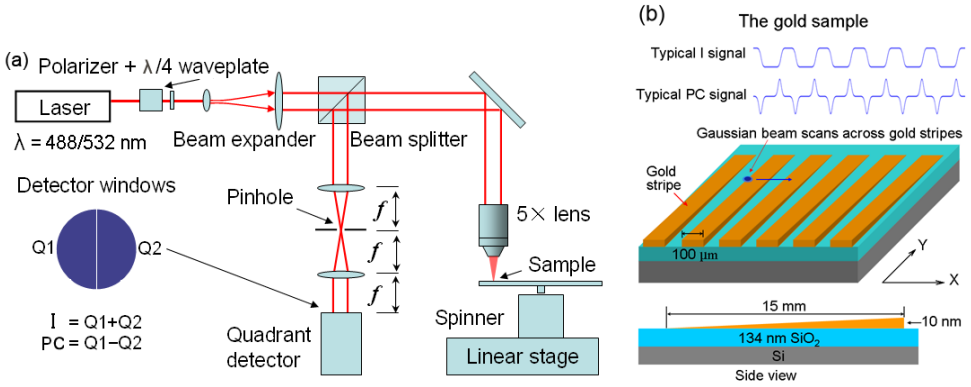

Fig. 1. Schematics of picometrology and the gold sample. (a) Picometrology measures the complex refractive index of ultra-thin films at single wavelengths at normal incidence. The reflected Gaussian beam forms an asymmetric diffraction pattern on the Fourier plane when scanning across film edges. By analyzing the intensity variation (I signal) and spatial asymmetry (PC signal) of the diffraction pattern with a split detector, full information is acquired of the complex refractive index calculation. (b) The gold sample is fabricated for the optical study for thicknesses in the range of 0~10 nm on a single chip. The gold effective thickness (measured mass per area divided by molecular mass volume density) increases from 0 to 10 nm along the –Y direction, and the gold film has a stripe pattern along the X direction to provide multiple film edges for the picometrology analysis.

Two-dimensional picometrology scanning was performed on the gold sample at wavelengths of 488 nm and 532 nm. Images of I and PC scans are shown in Fig. 2b and 2c. Normalization is performed by dividing the I and PC signal by the intensity of the reflected beam on the adjacent land of the substrate. As a demonstration, in Fig. 3a, the I and PC signals are extracted for 4 nm gold, and $\tilde{n}$ for gold is calculated at this thickness. Although the approximation in Eq. (1) is suitable to calculate $\tilde{n}$ when the thickness is much less than

#135785 - $15.00 USD Received 28 Sep 2010; revised 25 Oct 2010; accepted 26 Oct 2010; published 12 Nov 2010

the probe wavelength, to improve calculation precision, we used a rigorous computational transfer matrix method [13] to extract the precise $\tilde{n}$ from the data. The $\tilde{r}$ of the substrate ($\tilde{r} = -0.38 - 0.42i$ at 488 nm wavelength and $\tilde{r} = -0.19 - 0.46i$ at 532 nm wavelength), the film thickness d, and the I and PC responses are measured, hence we plot $\tilde{n} = n + ik$ on the complex plane to find a value of $\tilde{n}$ that satisfies both the I and PC responses. For each thickness there is a single curve on which all $\tilde{n}$ give a constant I response (which explains why reflectometry alone cannot determine the $\tilde{n}$). All $\tilde{n}$ satisfying the PC response form a separate curve. The intersection of the I and PC curves uniquely determines the target $\tilde{n}$ (Fig. 3b) at this thickness. By these means, $\tilde{n}$ of gold is calculated for any thickness less than 10 nm. The curves of $\tilde{n} = n + ik$ are shown in Fig. 3d. Gold with effective thickness below 10 nm is usually not a continuous medium but has the topology of heterogeneous clusters with a connectivity that goes through a percolation transition [14].

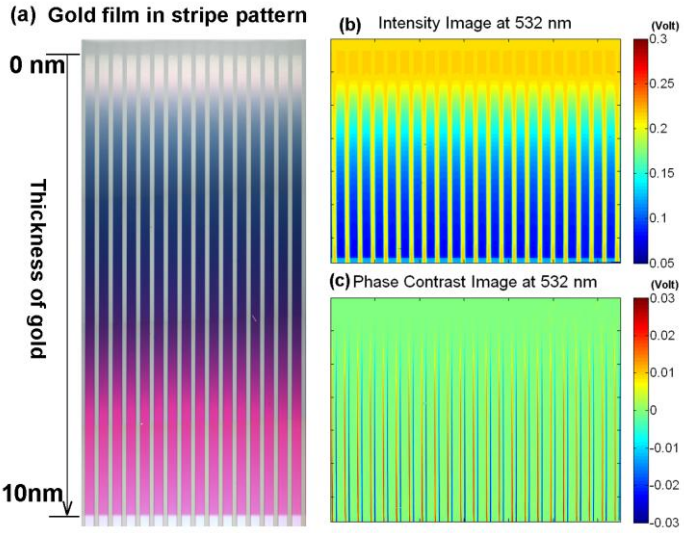

Fig. 2. Gold film pattern and I, PC response images. (a) Stripe-patterned gold film with thickness varying continuously from 0 to 10 nm on thermal oxide on silicon (134 nm SiO_2). The sample is prepared using a thermal metal evaporator in which the evaporation time is controlled by a stepper motor. The image is captured by microscope under white light. The color of the gold shows a rich transition within 10 nm (Real color). (b) and (c) show the images of the sample in the I and PC channels scanned by the picometrology system at 532 nm (Pseudo color).

#135785 - $15.00 USD Received 28 Sep 2010; revised 25 Oct 2010; accepted 26 Oct 2010; published 12 Nov 2010

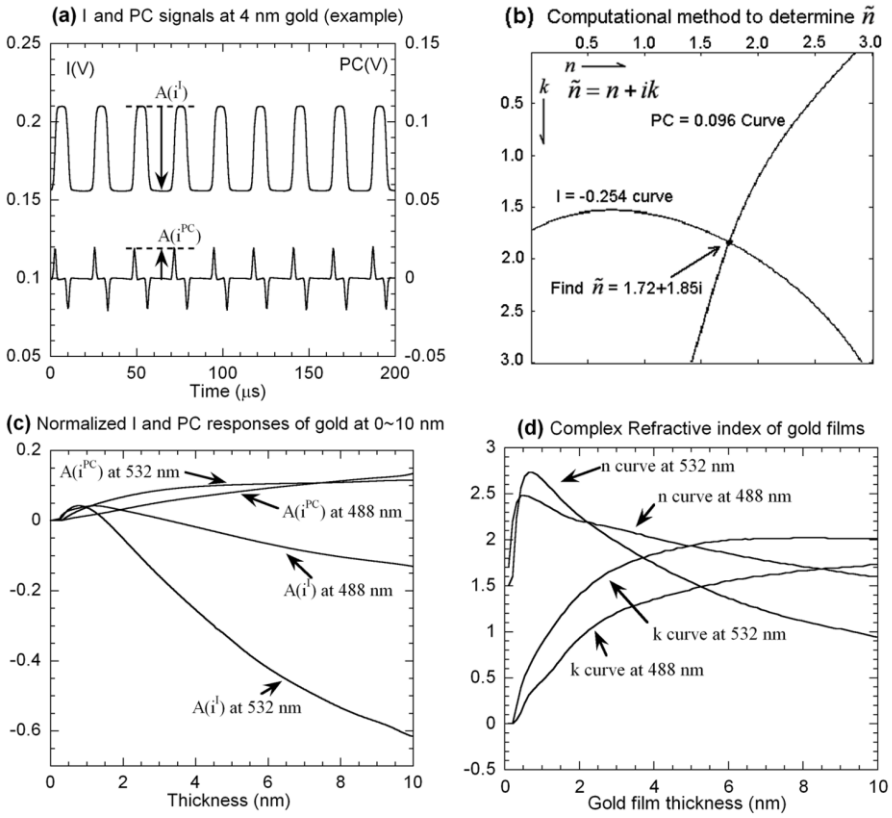

Fig. 3. Data processing to calculate refractive indices of ultra-thin gold. (a) One example of I and PC signals from 4 nm thick gold (one track taken from images Fig. 1b and 1c). The normalized amplitudes of both channels are acquired, and the refractive index of gold at this thickness can be calculated by Eq. (1). (b) The I response is satisfied by multiple $\tilde{n}$ which form a curve on the complex plane, and similarly for the PC response. The intersection point uniquely determines $\tilde{n}$ of the gold film. (c). Normalized amplitudes of I and PC responses of gold from 0 to 10 nm at 488 nm and 532 nm wavelengths. (d) The $\tilde{n}$ is calculated for gold films with 0~10 nm thicknesses at both 488 nm and 532 nm wavelengths.

The trajectory of the dielectric constant $\tilde{\varepsilon}_g = \varepsilon' + i\varepsilon'' = \tilde{n}^2$ across the complex plane, parameterized by the film thickness, is shown in Fig. 4 for the wavelengths 488 nm and 532 nm for which the collective plasmon contributions to the Drude response are small [7]. Three distinct regimes are observed in the $\tilde{\varepsilon}_g$ trajectories as film thickness decreases from 10 nm to 0.2 nm. In the first regime (gold thickness decreases from 10 nm to 2 nm), $\tilde{\varepsilon}_g$ evolves in a circular trajectory. In the second regime (gold thickness from 2 nm to 1 nm), $\tilde{\varepsilon}_g$ evolves in a linear trajectory. In the third regime (gold thickness from 1 nm to 0.2 nm), $\tilde{\varepsilon}_g$ evolves with the imaginary part approaching zero as the discontinuous film fragments completely into finely scattered clusters.

#135785 - $15.00 USD Received 28 Sep 2010; revised 25 Oct 2010; accepted 26 Oct 2010; published 12 Nov 2010

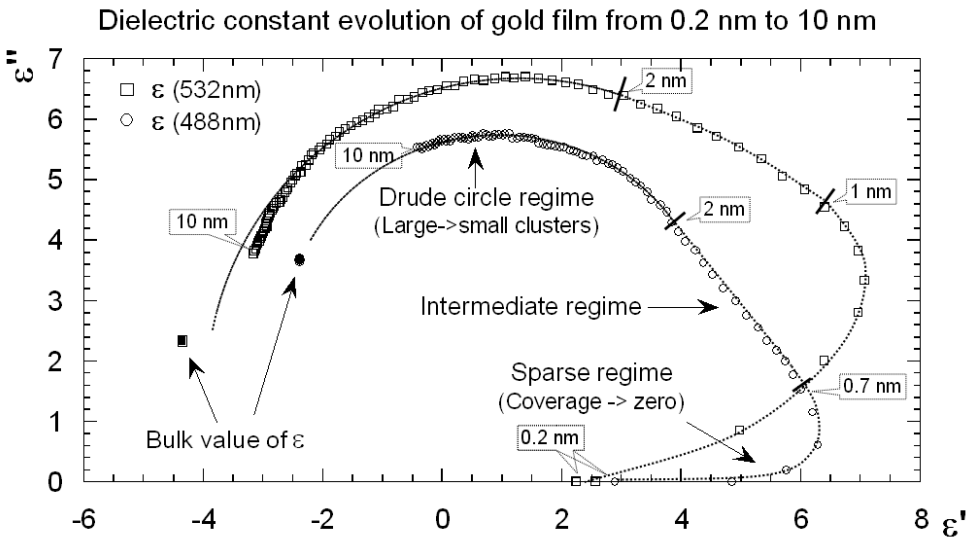

Fig. 4. The dielectric trajectories of gold film as the film thickness changes from 0.2 to 10 nm. The dielectric trajectory has three distinct regimes that originate from three types of gold topology: 1) Sparse regime (0.2 nm to 1 nm). In this regime, coverage of gold clusters goes from zero to 20%, and the imaginary part of $\tilde{\varepsilon}_g$ vanishes at ultra-low coverage. 2) Intermediate regime (1 nm to 2 nm) connecting the first and third regime. 3) Drude circle regime (2 nm to 10nm). In this regime, the effective dielectric constant of gold film $\tilde{\varepsilon}_g$ evolves along a circular trajectory (Drude circle). This pattern is predicted by the Drude equation as the size of the metal clusters increases above the electron mean free path.

3. Discussion

To interpret the $\tilde{\varepsilon}_g$ trajectory of ultra-thin gold, the microscopic topology of the film was analyzed by a Field-Emission scanning electron microscopy (SEM, Hitachi S-4800 Field Emission SEM). For instance, a gold film with a mass-equivalent thickness of a nanometer is a collection of isolated gold clusters. The size, shape (aspect ratio) and surface coverage of the gold clusters determines the effective dielectric constant. SEM imaging was performed to measure the surface coverage, aspect ratio and size of the gold clusters at thicknesses of 1, 2, 5 and 10 nm. The data and topology analysis are shown in Fig. 5, enabling us to interpret the evolution of $\tilde{\varepsilon}_g$.

#135785 - $15.00 USD Received 28 Sep 2010; revised 25 Oct 2010; accepted 26 Oct 2010; published 12 Nov 2010

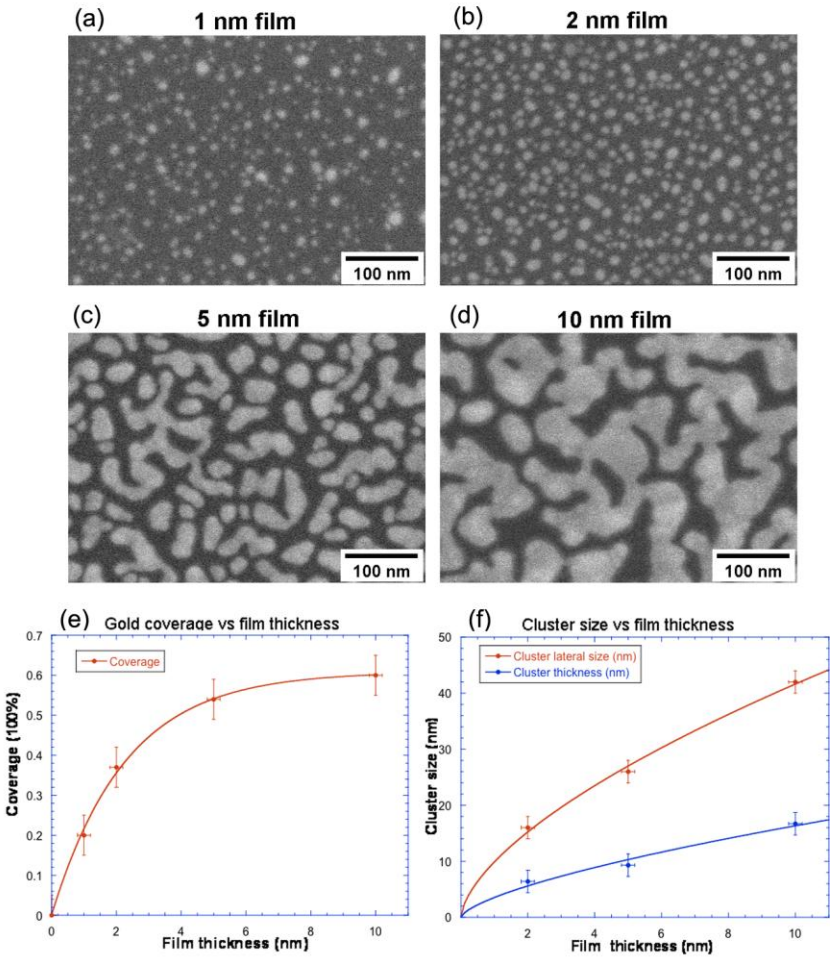

Fig. 5. SEM images of the gold samples and gold topology analysis. (a), (b), (c), (d) show the images of gold clusters at different mass-equivalent film thicknesses. (e) and (f) show Gold topology in terms of coverage, cluster lateral size and film thicknesses. The cluster height was calculated by dividing the average gold thickness by the coverage, and the cluster lateral size was calculated by auto-correlation analysis of the SEM images. Cluster coverage rapidly and almost linearly increases from 0 to 37% as the average thickness of gold film changes from 0 to 2 nm. The coverage increases at a much slower rate when film thickness grows beyond 3 nm. As a result, coverage increases from 54% to 60% as the gold thickness changes from 5 to 10 nm.

In the thinnest regime (mass-equivalent thickness 0.2 – 0.6 nm), the dipole density on the surface increases causing an increase of the real part of the dielectric constant as the gold clusters grow in lateral size up to 10 nm (4 nm in height) up to a surface coverage of 15%. Approximately at this size, the clusters begin to take on metallic character, and the dielectric trajectory reaches the turning point in the real part of the dielectric constant as the imaginary part increases rapidly. In the mid-thickness regime (mass-equivalent thickness 0.6 to 2 nm) the coverage increases from 15% up to 40%, as the lateral size of the clusters increases to 16 nm (6 nm height). The trajectory is approximately linear in this regime, with the real part decreasing and the imaginary part increasing.

In the thickest regime of the trajectory of $\tilde{\varepsilon}_g$ (Drude circle regime where gold thickness increases from 2 nm to 10 nm), the aspect ratio of gold clusters changes little as the coverage varies slowly (coverage above 50%), but the average lateral size of the gold clusters changes

#135785 - $15.00 USD Received 28 Sep 2010; revised 25 Oct 2010; accepted 26 Oct 2010; published 12 Nov 2010

from 16 nm to 42 nm (6 nm to 16 nm in height). The cluster size is the major factor determining the effective $\tilde{\varepsilon}_g$ of the gold film in this regime causing $\tilde{\varepsilon}_g$ to evolve in a circular trajectory in Fig. 4 as the film thickness increases. This phenomenon is caused by gradual deconfinement of the free electrons in gold clusters caused by the increasing cluster size. According to the Drude theory [15,16], the $\tilde{\varepsilon}_g$ of nanoscale gold structures is described as

$$\varepsilon_g = \varepsilon_{bound} - \frac{\omega_p^2}{\omega^2 + i\Gamma(d)\omega}, \tag{2}$$

where ω_p is the bulk plasmon frequency, ω is the probe light angular frequency, ε_{bound} is the dielectric constant contributed by bound electrons, and $\Gamma(d)$ is the collision frequency of free electrons. $\Gamma(\infty)$ is a constant (bulk value), but when the cluster size is on the order of the electron mean free path (25 nm in Au [17]), $\Gamma(d)$ increases due to surface collisions. In Ref [18], the approximate behavior was parametrized by $\Gamma = \Gamma(bulk) + 2\pi v_F / s$ where v_F is the Fermi velocity of free electrons and s is the radius of a metal nano-particle. Therefore, $\tilde{\varepsilon}_g$ evolves in a circular trajectory, called the Drude Circle, as $\Gamma(d)$ varies and ω is held constant. This is a direct consequence of the equation

$$\left| \tilde{\varepsilon}_g - (\varepsilon_{bound} - \frac{\omega_p^2}{2\omega^2}) \right| = \left| \left(\frac{-1 + i\Gamma/\omega}{1 + i\Gamma/\omega} \right) \frac{\omega_p^2}{2\omega^2} \right| = \frac{\omega_p^2}{2\omega^2} \tag{3}$$

that describes a parametric circular trajectory for $\Gamma \in [\Gamma_{Bulk}, \infty]$.

The radius of this circle on the complex plane is $\omega_p^2 / 2\omega^2$ centered at $\varepsilon_{bound} - \frac{\omega_p^2}{2\omega^2}$. The Drude circle describes the parametric trajectory of $\tilde{\varepsilon}_g$ for metal clusters as Γ varies. By fitting the data in the first regime on Fig. 4, the radii are found to be 3.8 at 488 nm and 5.2 at 532 nm, giving a plasmon energy of 7.3 eV and $\varepsilon_{bound} \approx 6 + 1.6i$. The plasmon frequency of bulk Au is between 7.5 – 8.5 eV in [19–21]. Therefore, the Drude equation is consistent with our experimental results. The turning point in the imaginary part of the dielectric constant (the apex of the trajectory) occurs when the free electron scattering rate equals the optical angular frequency $\Gamma = \omega$. To study Drude behavior, previous approaches tuned the frequency ω while treating Γ as a constant. Here, we observe the Drude circle for the first time by using the graded-thickness gold sample combined with picometrology in a single photonic state, allowing $\Gamma(d)$ to vary parametrically and to observe $\tilde{\varepsilon}_g$ at different gold thicknesses, while keeping ω constant (constant radius on the complex plane).

Our experiment tracks the metal-to-insulator (I/M) transition of gold film from an optical perspective. The geometric percolation threshold is reached when a single giant cluster spans the probe scale, which occurs around a mass-equivalent thickness of 7 nm in our samples. Therefore, although the geometric percolation thickness is well within the Drude circle, there is no measurable feature or deviation from the circular Drude trajectory in that thickness range. For optical frequencies, continuous percolation across long-range gold clusters has little or no influence on the optical properties of a gold film. There is evidence [22] in the microwave region (4.9 GHz, 60 mm wavelength) that the conductivity of a gold film decreases abruptly below a thickness of 8 nm, which is consistent with the percolation threshold. Higher-frequency infrared light ($\lambda = 24\ \mu m$) displayed a transmission anomaly at the thinner value of 2 nm [3], which is where, in our results, the Drude circle commences

#135785 - $15.00 USD Received 28 Sep 2010; revised 25 Oct 2010; accepted 26 Oct 2010; published 12 Nov 2010

(metallic optical behavior) as a continuation of the mid-thickness regime of the dielectric trajectory.

4. Conclusion

In conclusion, we have measured the dielectric trajectory on the complex plane of thermally-evaporated gold on silica at the wavelengths 532 nm and 488 nm with mass-equivalent gold film thickness as the parametric variable. Picometrology is able to extract the full complex dielectric trajectory using a single-wavelength measurement without polarization control and at normal incidence. We extracted $\tilde{\varepsilon}_g$ of gold films with arbitrary thickness in the range of 0.2 nm to 10 nm, and demonstrated that the $\tilde{\varepsilon}_g$ trajectory traces out the Drude circle for mass-equivalent thicknesses greater than 2 nm.

Acknowledgement

This project is sponsored by a grant from the 21st Century Fund of the Indiana Economic Development Corporation. We sincerely thank Dr. Vladimir Shalaev for fruitful discussions. We also thank Jacob Millspaw and Chris Petrovitch for help processing the gold samples.

#135785 - $15.00 USD Received 28 Sep 2010; revised 25 Oct 2010; accepted 26 Oct 2010; published 12 Nov 2010